Vacuum 168 (2019) 108801

Contents lists available at ScienceDirect

Vacuum

journal homepage: www.elsevier.com/locate/vacuum

WC-Fe layer with high volume fraction and fracture toughness on cast iron fabricated by in situ solid-phase diffusion

Lisheng Zhong[a,b,*], Chao Deng[a,b], Xi Zhang[a,b,c], Haiqiang Bai[a,b,d], Jianlei Zhu[a,b], Zhengxin Lu[a,b,e], Yunhua Xu[a,b,d]

[a] School of Material Science and Engineering, Xi'an University of Technology, Xi'an, 710048, PR China
[b] International Research Center for Composite and Intelligent Manufacturing Technology, Xi'an University of Technology, Xi'an, 710048, PR China
[c] School of Materials and Chemical Engineering, Xi'an Technological University, Xi'an, 710021, PR China
[d] School of Chemistry and Chemical Engineering, Yulin University, Yulin, 719000, PR China
[e] Xi 'an Zhitong Automation Technology Ltd. Co., Xi'an, 710048, PR China

ARTICLE INFO

Keywords:
WC-Fe layer
In situ solid-phase diffusion
Fracture toughness

ABSTRACT

A WC-Fe layer on cast iron was fabricated by in situ solid-phase diffusion method near the Fe–W–C ternary eutectic temperature. The phase composition and microstructure of the WC-Fe layer were studied by XRD, SEM, and EBSD. Meanwhile, the fracture toughness (K_{IC}) of the layer was tested and calculated by indentation method. The results showed that the main phases were WC and α-Fe on the surface WC-Fe layer after removing excess tungsten plate, while the volume fraction of WC reached up to 86%. WC/α-Fe/WC laminar structure was formed due to the Fe atoms continued the stacking sequence of WC when they diffuse into the growth front. The cross-section microstructure showed evident gradient distribution characteristics. With the increase in holding time from 5 min to 135 min, the amount of Fe_6W_6C decreased, and the particle size of WC increased from 1.9 μm to 3.1 μm in the average. The K_{IC} of the WC-Fe layer was 7.45 MPa $m^{0.5}$, while the average hardness of WC-Fe layer was 16.88 GPa. The excellent K_{IC} of the WC-Fe layer when the volume fraction of WC was extremely high due to WC-Fe-WC laminar structure, was formulated by the incorporation of WC-layered growth and Fe atom stacking mode.

1. Introduction

Tungsten carbide reinforced steel–iron matrix surface composites are widely used in mining, metallurgy, and electric power due to their high strength and good wear resistance properties [1]. The main reason for their excellent wear resistance is that the tungsten carbides, which shows high hardness (22 GPa (0001) crystal plane), elastic modulus (620–720 GPa), and melting point (2870 °C), are added into the matrix [2,3]. Many methods have been used to prepare the tungsten carbide-reinforced steel–iron matrix surface composites, but in situ methods showed considerable potential and advantages. The interface between carbide and steel–iron matrix is generally clean and compatible. The in situ synthesis of carbide is thermodynamically stable and shows decreased gradation in high-temperature applications. The interfacial bonding force between carbide and metal is strong. Niu et al. [4] designed WC-reinforced Fe-based surface composites by centrifugal casting. Experimental results showed that the surface composites are compact and consist mainly of primary WC and fine secondary WC as the reinforcing phases. Compared with unreinforced cast iron, the composite has high resistance to polish wear and microploughing. Wang et al. [5] applied precursor carbonization and plasma cladding method to prepare the W–C compound powder to perform the in situ synthesis of the WC phase in a Fe-based alloy coating. The results revealed that fine and obtuse WC particles are generated and distributed in a Fe-based alloy coating. Several other in situ techniques such as laser cladding [6–9], Ar arc cladding [10], gas tungsten arc welding [11], pulsed-arc plasma deposition [12], and pulsed reactive magnetron sputtering [13], have been used to prepare tungsten carbide reinforced steel–iron matrix surface composites. The volume fraction of the tungsten carbide in the matrix need to be observed. Not all studies considered the volume fraction of carbide as a necessary parameter, although it has a considerable influence on the mechanical properties of composites. In general, the wear resistance, hardness, and compressive strength of the composites increase with the increase in the volume fraction of tungsten carbide, while the toughness and yield strength of the composite may decrease when the fraction of carbide increases to

* Corresponding author. Xi'an University of Technology, No. 5 Jinhua Road, Xi'an, 710048, China.
E-mail address: zhonglisheng@xaut.edu.cn (L. Zhong).

https://doi.org/10.1016/j.vacuum.2019.108801
Received 12 June 2019; Received in revised form 3 July 2019; Accepted 3 July 2019
Available online 04 July 2019
0042-207X/

Table 1
The volume fraction of tungsten carbide in the matrix which prepared by typical in situ methods.

Reinforcement	In situ Methods	Matrix	Volume Fraction (%)	References
WC, W_2C	laser melt injection (LMI)	cast duplex stainless steel	10	[15]
WC, Al_2O_3	cast-infiltration	iron casting with 12% Cr	30	[16]
WC	laser cladding	mild steel	71	[9]
WC	in situ solid-phase diffusion	gray cast iron	> 80	[14]

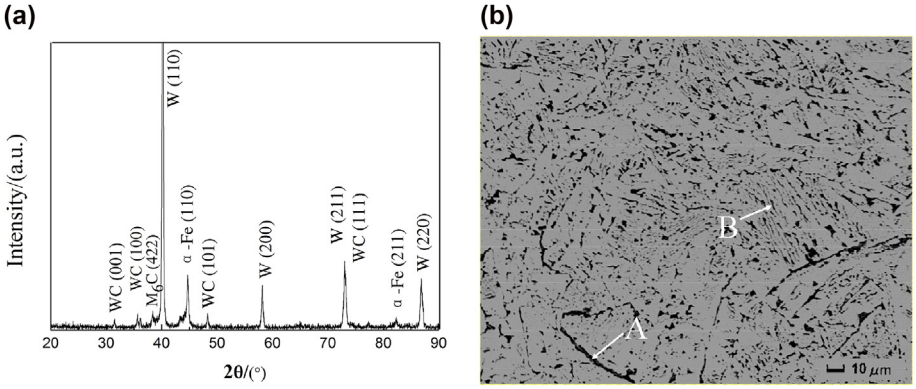

Fig. 1. The XRD results (a) and SEM images (b) of the surface WC-Fe layer on cast iron at 1085 °C for 135 min.

some extent [5,8]. Table 1 shows the volume fraction of tungsten carbide in the matrix, which is prepared by typical in situ methods. The volume fraction of the tungsten carbide particle on Ni-based composite coating on mild steel by laser cladding in situ synthesis reaches 71% [9]. In our previous works, tungsten carbide-reinforced Fe-based surface composites were prepared by in situ solid-phase diffusion with the volume fraction of up to 80% [14]. The volume fraction of tungsten carbide reaches an extremely high value in the surface composite and obtained excellent hardness and wear resistance. However, to the authors' knowledge, no results about toughness, which also has important influence on actual application, have been reported.

In this paper, a WC-Fe layer with high volume fraction and high fracture toughness (K_{IC}) on cast iron was fabricated by in situ solid-phase diffusion method with low temperature near the Fe–W–C ternary eutectic temperature. The phase composition and microstructure of the WC-Fe layer were studied by XRD, SEM, and EBSD, while the K_{IC} of the layer was tested and calculated by indentation method. The toughening mechanism of the WC-Fe layer with high volume fraction on cast iron were analyzed.

2. Experimental

2.1. Materials and preparation

The starting materials were tungsten plate with 99.7 wt% purity and gray cast iron, which were used as the W and C sources for the in situ synthesis of WC grain on surface of cast iron, respectively. The chemical composition (wt%) of gray cast iron was Fe-3.45C-0.56Si-0.268Mn-0.224P-0.024S. The tungsten carbide-reinforced Fe-based surface composites were prepared by in situ solid-phase diffusion method. The specimen was subjected to heat treatment in a horizontal tube furnace (GSL 1400, Hefei Kejing Materials Technology Co. Ltd., China) at 1085 °C for 15 and 135 min with a modest flow of argon gas (5 mL/min) and cooled down naturally to room temperature. The detail experimental methods and procedures have been described in our previous work [14].

2.2. Analysis methods

The specimens of surface and cross-section WC-Fe layer on gray iron were ground and polished for phases compositional analysis and microstructure observation. The XRD data were recorded in the 2θ ranging from 20° to 90° on a PW 1730 X-ray diffractometer (Philips, The Netherlands) with monochromatic CuK_α radiation at 40 kV and 40 mÅ. The microstructure of specimens was observed by SEM (JEOL, JSM-5800, Japan) equipped with an energy dispersive X-ray spectrometer (EDS). The phase, grain morphology, and size were characterized by EBSD (ZEISS, Germany). The volume fraction of the WC in the layer was determined by image statistical analysis method, which was introduced elsewhere [17]. The hardness and elastic Young's modulus of the WC-Fe layer were measured by nanoindentation under 450 mN load. The K_{IC} of the specimen was calculated and determined using Niihara's equation and the Vickers indentation by microhardness tester (HXD-1000, Shanghai) that consisted of a square-based pyramidal diamond indenter with a 136° angle between two opposite faces and 2 kg load.

3. Results and discussion

3.1. Phase and microstructure of surface WC-Fe layer on cast iron

Fig. 1a shows XRD result of the surface WC-Fe layer on cast iron when the holding temperature and time were 1085 °C and 135 min, respectively. The figure shows that the main phases were WC and α-Fe, and no other W, iron carbide, or ferrotungsten phases were observed. The microstructure of the surface WC-Fe layer was investigated by SEM, as shown in Fig. 1b. A number of grey irregular grains was distributed on dark matrix. The EDS results showed that the grey irregular grains were composed of C and W in a ratio of almost 1:1, and the dark matrix was composed with Fe. Combined with XRD results, the results showed that compact tungsten carbide was distributed on the α-Fe matrix. The volume fraction of tungsten carbide was up to 86%, which was calculated by Image-Pro Plus software. Compared with laser melt injection, cast infiltration, and laser cladding, in situ solid-phase diffusion method can obtain high carbide volume fraction (Table 1). The α-Fe matrix existed between points A and B internally in irregular tungsten carbide particles, which showed WC/α-Fe/WC laminar structure.

In the in-depth observation and analysis of the laminar structure, the EBSD analysis of the microstructure of the surface WC-Fe layer at 1085 °C for 135 min is shown in Fig. 2. Phase and all Euler maps in Fig. 2 a and b showed that α-Fe phase existed not only among WC

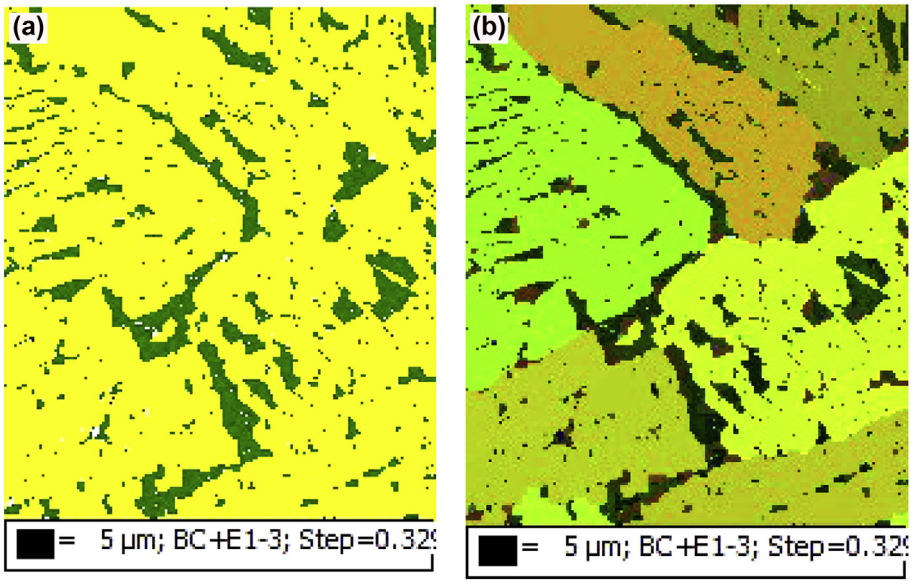

Fig. 2. Phase map (a) and all Euler map (b) of the microstructure of the surface WC-Fe layer at 1085 °C for 135 min (WC in yellow; α-Fe in green). (For interpretation of the references to colour in this figure legend, the reader is referred to the Web version of this article.)

particles but also within WC particles. This result further confirmed that the surface WC-Fe layer comprised WC/α-Fe/WC laminar structure, which was consistent with SEM image results. According to pole figures, the distribution of WC had a certain orientation concentration, especially on the {0001} crystal plane. The extreme density intensity (MUD) of WC reached 43.59, thereby indicating that WC has preferred orientation.

The WC/α-Fe/WC laminar structure formation was closely related to the in situ nucleation and growth of WC. WC is a simple hexagonal structure with $a = 0.2906$ nm, $c = 0.2837$ nm, $c/a = 0.967$. The W and C atoms were located on (0, 0, 0) and (1/3, 2/3, 1/2), respectively, which determined the initial grain morphology. During growth, the in situ WC will change its shape to minimize the surface energy, according to Gibbs–Wulff theory [18]. In the Fe–Ni–W–C alloy system, the morphology evolution of in situ WC grains followed the order sphere-like→icosahedron→octahedron→truncated-octahedron→flat-tri prism [19]. Flat-tri prism is a stable morphology of WC grains. From another point of view, the evolution rule of WC morphology and crystal face can be explained by classical periodic bond chain (PBC) theory. The *F*, *S*, and *K* faces for the simple hexagonal structure of the in situ WC are {0001}, $\{01\bar{1}0\}$, and $\{10\bar{1}0\}$, respectively. Hence, {0001} is the most stable face, while $\{10\bar{1}0\}$ disappears finally.

In present work, the laws above will not change, but at least two points, that is, interface structure and stability between WC and α-Fe, should be considered. The interface structure between WC and α-Fe was determined by mismatch (δ), as follows:

$$\delta = (a_{WC}\text{-}a_{\alpha\text{-Fe}})/a_{\alpha\text{-Fe}} \quad (1)$$

where a_{WC} and $a_{\alpha\text{-Fe}}$ are the lattice constants of WC and α-Fe, respectively. When $\delta < 0.05$, the interface structure between WC and α-Fe is the coherent interface. When $0.05 < \delta < 0.25$, the interface structure is the semicoherent interface. When $\delta > 0.25$, the interface structure is the incoherent interface. The a_{WC} and $a_{\alpha\text{-Fe}}$ values were 2.906 and 2.866 Å, respectively, and the δ value was 0.01376, which was < 0.05. Hence, the interface structure between WC and α-Fe is the coherent interface. For interface stability between WC and α-Fe, Gao et al. studied the stability and bonding of Fe/WC interfaces using first-principles calculations [20]. For HCP stacking geometry interface, Fe atoms showed that the stacking sequence of WC, C-HCP, and W-HCP interfaces had strong covalency and metallic bonds, respectively.

As shown above, the in situ WC growth followed Gibbs-Wulff and PBC theories. Fe atoms participate in the WC growth process because the Fe atoms continued the stacking sequence of WC when they diffused into the growth front. The WC-Fe-WC laminar structure was formulated by the incorporation of WC-layered growth and Fe atom stacking mode.

3.2. Cross-section WC-Fe layer phase and microstructure

The XRD result of the cross-section WC-Fe layer on cast iron is shown in Fig. 3a. The figure shows that the main phases were W, Fe_6W_6C, WC, and α-Fe. Meanwhile, as shown in the cross-section SEM image in Fig. 3b, c, and d, the W, Fe_6W_6C, WC, and α-Fe phases followed the order from the surface to the center (Fig. 3b). Hence, the phases of the cross-section WC-Fe layer on cast iron showed evident gradient distribution characteristics. Between tungsten plate and compact tungsten carbide layer, Fe_6W_6C with only several micrometers was present (zone E in Fig. 3c). This thin Fe_6W_6C layer can be easily broken when removing excess tungsten plate. Hence, no diffraction peak is observed in the XRD result for the surface WC-Fe layer (Fig. 1a). Irregular or triangular prism WC particles were observed close to the matrix (Fig. 3d). The WC grain showed that the irregular or triangular prisms were developed via layer-by-layer growth characteristics, which were reported in other literature [19,21]. Along the ⟨0001⟩ direction, many lamellar triangular structures were stacked vertically step by step in the descending order of the basal facets {0001}, and only few triangular WC growth units were stacked separately [19].

To observe the microstructure of the cross-section WC-Fe layer, we performed EBSD analysis. Fig. 4 shows the EBSD results of the surface WC-Fe layer at 1085 °C for 15 and 135 min. Regardless of the holding time, phase and all Euler maps showed that a Fe_6W_6C layer with only several micrometers of thickness was actually present (zone F in Fig. 4a and G in Fig. 4c), which was consistent with SEM image (zone E in Fig. 3c). For the holding time of 15 min, the thickness of the compact WC-Fe layer was only in the range of 5–10 μm, and no gradient distribution characteristics were present. Meanwhile, according to pole figures, the distribution of WC had a certain orientation concentration, especially on {0001} crystal plane. The MUD of the WC reached 59.09. The average grain size of WC in the layer was also approximately 1.9 μm. For the prolonged holding time of 135 min, the thickness of the Fe_6W_6C layer was thinner than that holding in 15 min, while the thickness of the compact WC-Fe layer increased to 55–60 μm. The average grain size of the WC in the layer increased up to 3.1 μm. The

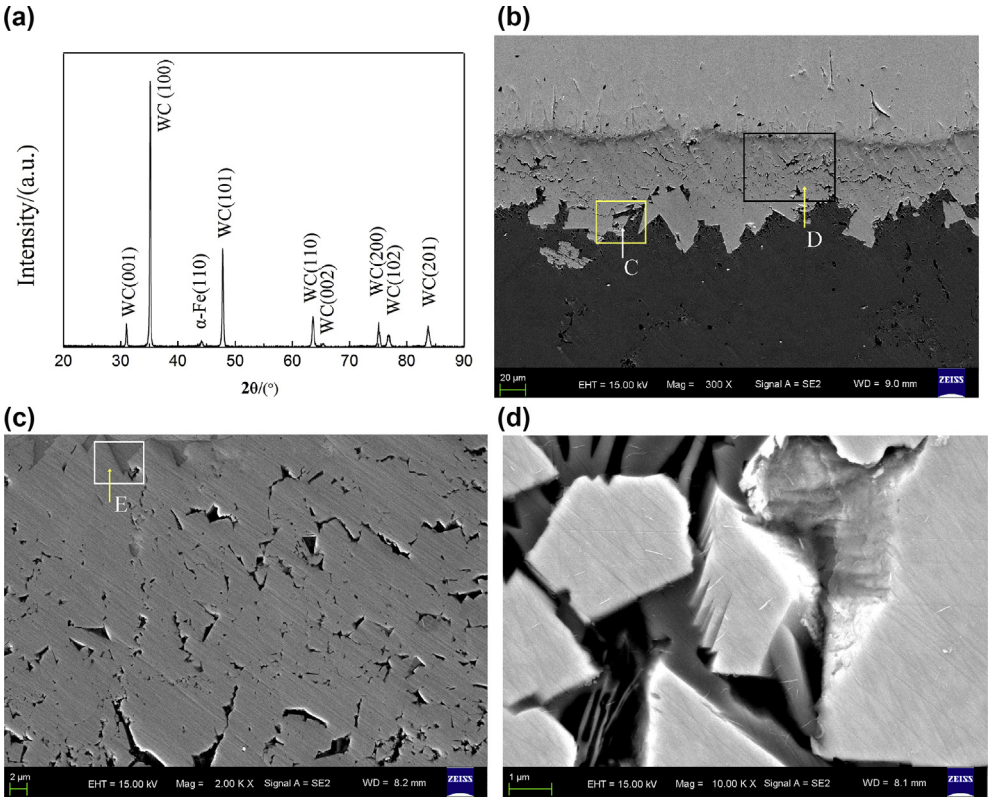

Fig. 3. The XRD results (a) and SEM images (b, c, d) of cross section WC-Fe layer at 1085 °C for 135 min.

grain size of the WC gradually decreased from the interface between W plate and Fe_6W_6C layer to matrix. Hence, the WC distribution in the cross-section WC-Fe layer presents the feature of evident gradient distribution when holding for a certain duration.

The formation process and mechanism of the WC-Fe layer were discussed in detail elsewhere, and the main processes included desolventization, diffusion, and in situ reactions [14]. The mechanism of the WC gradient distribution in the WC-Fe layer can be described as C and

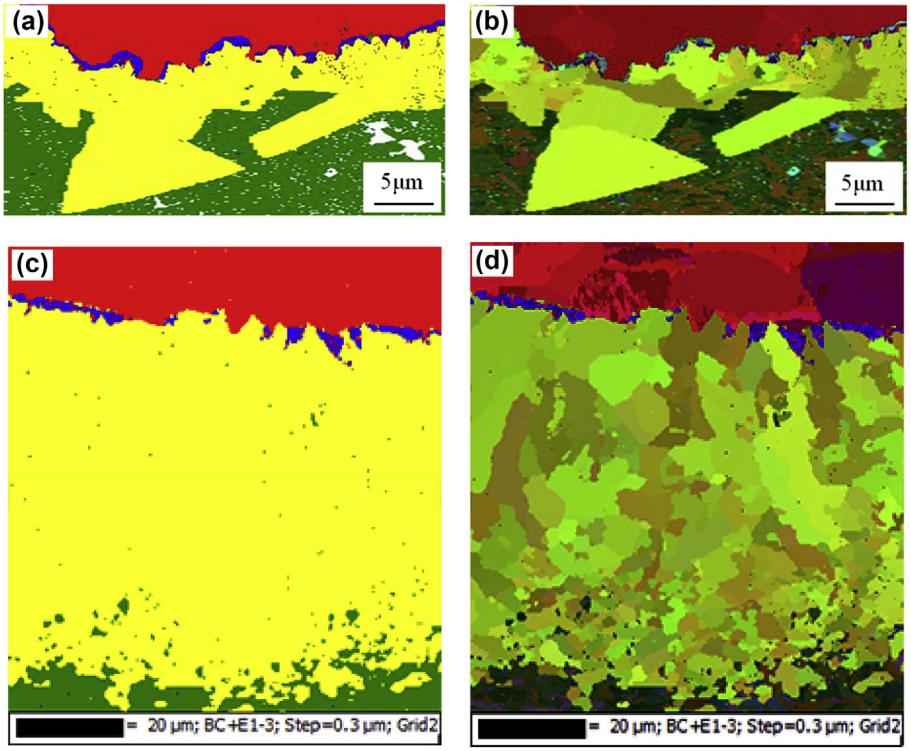

Fig. 4. Phase map (a, c) and all Euler map (b, d) of the surface WC-Fe layer at 1085 °C for 15 and 135 min (W in red; WC in yellow; α-Fe in green; Fe_6W_6C in blue). (For interpretation of the references to colour in this figure legend, the reader is referred to the Web version of this article.)

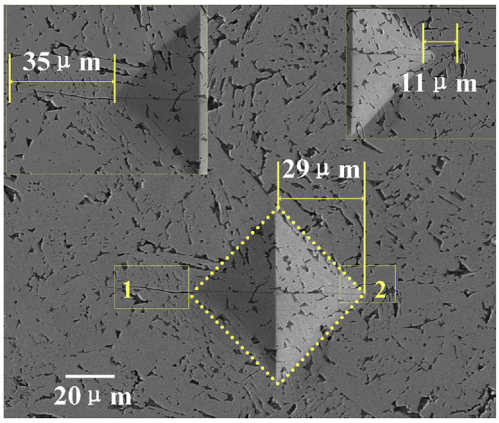

Fig. 5. Micrograph of the Vickers indentation and crack for the surface WC-Fe layer on cast iron.

Fe diffusion from matrix to W plate. The WC grains that were in situ synthesized by W and C were dispersed by Fe at 1085 °C. Hence, C and Fe pass through the WC-Fe layer easily. However, the complex cubic structure of Fe_6W_6C narrowed the atom diffusion path [22]. C, Fe, and W were difficult to diffuse through the Fe_6W_6C layer with long-range diffusion; only short-range diffusion occurred, especially for Fe and W. When the treatment time was prolonged, the WC-Fe layer thickness increased. At the same time, decreased C atoms reached the interface between Fe_6W_6C layer and WC-Fe layer. On the one hand, the WC nucleation rate decreased with the decrease in C content. On the other hand, low C environment promoted WC growth. In brief, the grain size of WC close to interface between the Fe_6W_6C and WC-Fe layers was large, while that of the WC that was close to matrix was small.

3.3. Hardness and K_{IC} of WC-Fe layer on cast iron

Describing the hardness distribution of cross-section WC-Fe layer on cast iron was no longer necessary because the Vickers hardness profiles from the interface between tungsten plate and WC-Fe layer to the matrix have been analyzed in detail in a previous work [14]. However, the surface hardness was not described, which was determined by the nanoindentation method here. Meanwhile, the K_{IC} of the surface WC-Fe layer on cast iron was tested by Vickers indentation and calculated according to the Niihara's equation [23]. The nanoindentation results showed that the average hardness and elastic Young's modulus of WC-Fe layer on cast iron were 16.88 and 563.77 GPa, which were slightly lower than the theoretical values (22 GPa in hardness and 620–720 GPa in elastic modulus), respectively. Fig. 5 shows a micrograph of the Vickers indentation and crack for the surface WC-Fe layer on cast iron. The results showed that the value of l/a was 0.793, which was in the range of 0.25–2.5, thereby belonging to the Palmqvist crack type [24]. According to the Niihara's equation, the K_{IC} was described, as follows:

$$K_{IC} = 0.018\ H^{0.6}\ E^{0.4}\ a\ l^{-0.5}\ (0.25 < l/a < 2.5) \quad (2)$$

where H is the hardness in GPa; E is the elastic Young's modulus in GPa; a and l are the indentation and crack characteristic dimension (μm), respectively, as shown in Fig. 5.

Through calculation, the K_{IC} of the surface WC-Fe layer was 7.45 MPa $m^{0.5}$, which was higher than that of compact TaC–Fe layer on cast iron with similar volume fraction, with the K_{IC} of 6.63 MPa $m^{0.5}$ [23]. The existence of the α-Fe phase and WC/α-Fe/WC laminar structure was the main reason for decrease in WC-Fe layer brittleness.

4. Conclusion

For carbide reinforced steel-iron-matrix composites, lots of works show that the wear resistance and compressive strength of the composites increase with the volume fraction of carbide increase, while the toughness and yield strength of the composite may decrease when the fraction of carbide increases to some extent. In this paper, WC-Fe layer with high volume fraction and high frcture toughness on cast iron was fabricated by in situ solid-phase diffusion method with low temperature (1085 °C). On the surface, the main phases are WC and α-Fe, while the volume fraction of WCreached up to 86%. WC/α-Fe/WC laminar structure was formed due to Fe atoms continue the stacking sequence of WC when they diffuse into the growth front. On the cross section, the main phases are W, Fe_6W_6C, WC and α-Fe, which come in the order from the surface to the centre. With the increase in holding time from 5 min to 135 min, the amount of Fe_6W_6C decreases, and the particle size of WC increases from 1.9 μm to 3.1 μm in the average. The K_{IC} of WC-Fe layer is 7.45 MPa $m^{0.5}$, while the average hardness of WC-Fe layer is 16.88 GPa. The excellent K_{IC} of the WC-Fe layer on cast iron when the volume fraction of WC was extremely high due to the fact that the WC-Fe-WC laminar structure was formulated by the incorporation of WC-layered growth and Fe atom stacking mode.

Acknowledgements

The authors gratefully acknowledge the Key-point Research and Invention Program of Shaanxi Province (grant no. 2017ZDXM-GY-043) and the funding support of the International Research Center for Composite and Intelligent Manufacturing Technology (grant no. 2018GHJD-17) and Innovation Capability Support Program of Shaanxi Province (grant no. 2019-TD019).

References

[1] O. Hugh, Pierson. Handbook of Refractory Carbides and Nitrides [M], Noyes Publications, New Jersey, 1996.
[2] R. Koc, S.K. Kodambaka, Tungsten carbide (WC) synthesis from novel precursors, J. Eur. Ceram. Soc. 20 (11) (2000) 1859–1869.
[3] Schwarzkopf Paul, Richard Kieffer, Leszynski Werner, Benesovsky Fritz, Refractory Hard Metals: Borides, Carbides, Nitrides, and Silicides [M], Macmillan, 1953.
[4] L. Niu, Y. Xu, X. Wang, Fabrication of WC/Fe composite coating by centrifugal casting plus in situ synthesis techniques, Surf. Coating. Technol. 205 (2) (2010) 551–556.
[5] Miqi Wang, Zehua Zhou, Lintao Wu, Ying Ding, Zehua Wang, Characterization and in-situ formation mechanism of tungsten carbide reinforced Fe-based alloy coating by plasma cladding, Int. J. Minerals. Metal. Mater. 25 (4) (2018) 439–443.
[6] Xizhang Chen, Ke Hu, Qibing Yuan, Microstructure and performance of WC reinforced Fe-based composite coating synthesized in situ produced by laser cladding, China. Surface. Eng. 29 (4) (2016) 118–124 (In Chinese).
[7] Wenge Li, Guangjun Zhang, Jun Li, Cladding of WC-Cr_3C_2 cermet coating by laser controlled reactive synthesis, Key Eng. Mater. 368–372 (2008) 1872–1875.
[8] Yingying Chen, Wenge Li, Laser cladding in situ tungsten carbide reinforced ferrous matrix surface composites, Adv. Mater. Res. 189–193 (2011) 771–776.
[9] Da Shu, Zhuguo Li, Ke Zhang, Chengwu Yao, Dayong Li, Youlu Yuan, Zhenbang Dai, Phase constituents and growth mechanism of laser in situ synthesized WC reinforced composite coating with W-C-Ni system, J. Mater. Res. 32 (3) (2017) 557–565.
[10] Yifeng Xiao, Ming Tan, Lingli Peng, Jianxun Gong, Yuehui He, In situ synthesized WC particles reinforced Fe-based composite coating by argon arc cladding with tungsten powder, Adv. Mater. Res. 712–715 (2013) 378–381.
[11] Y.F. Xiao, H. Du, X.F. Li, Y.F. Xu, L. Wu, Y.H. He, In situ synthesis of WC ceramic particle reinforced composite coating by GTAW, Mater. Res. Innov. 19 (S9) (2015) 314–317 (2015 International Conference on Materials Science (ICMS2015)).
[12] R. Ospina, H.A. Castillo, V. Benavides, et al., Influence of the annealing temperature on a crystal phase of W/WC bilayers grown by pulsed arc discharge, Vacuum 81 (3) (2006) 373–377.
[13] A. Czyzniewski, Optimising deposition parameters of W-DLC coatings for tool materials of high speed steel and cemented carbide, Vacuum 86 (12) (2012) 2140–2147.
[14] L. Zhong, X. Zhang, X. Wang, Yunhua Xu, Hong Wu, Yonghong Fu, Growth kinetics of WC-Fe layer formed at the surface iron during solid-phase diffusion, Ceram. Int. 42 (15) (2016) 16941–16947.
[15] A.M. Do Nascimento, V. Ocelík, M.C.F. Ierardi, J. Th M. De Hosson, Microstructure of reaction zone in WC_p/duplex stainless steels matrix composites processing by laser melt injection, Surf. Coating. Technol. 202 (10) (2008) 2113–2120.
[16] Daxin Zeng, Janyong Liu, Yuanhao Zhang, Fe-WC surface composites produced by reactive cast-infiltration, China Foundry 1 (2) (2004) 138–140.
[17] Lisheng Zhong, Yunhua Xu, Xiaojie Liu, Fangxia Ye, Study on NbC particulate-reinforced iron matrix composite produced in situ, J. Mater. Sci. 46 (2011) 2814–2819.

[18] J.K. Lee, H.I. Aaronson, Application of the modified Gibbs-Wulff construction to some problems in the equilibrium shape of crystals at grain boundaries, Scripta Metall. 8 (1974) 1451–1460.
[19] Youlu Yuan, Zuguo Li, Growth mechanism of in-situ WC grain in Fe-Ni-W-C alloys system, J. Alloy. Comp. 738 (2018) 379–393.
[20] Yefei Li, Yimin Gao, Bing Xiao, Min Ting, Shengqiang Ma, Dawei Yi, Theoretical calculations on the adhesion, stability, electronic structure, and bonding of Fe/WC interface, Appl. Surf. Sci. 257 (2011) 5671–5678.
[21] Zhong Yang, L. Leon, Shaw, Growth mechanisms of WC in WC–5.75 wt% Co, Ceram. Int. 37 (8) (2011) 3591–3597.
[22] XiaoYu Chong, YeHua Jiang, Rong Zhou, Hong Zhu, Feng Jing, Electronic structure, anisotropic elastic and thermal properties of the η phase Fe_6W_6C, Comput. Mater. Sci. 108 (2015) 205–211.
[23] Ke Song, Yunhua Xu, Nana Zhao, Lisheng Zhong, Shang Zhao, Liuliu Shen, Juan Wang, Evaluation of fracture toughness of tantalum carbide ceramic layer: a Vickers indentation method, J. Mater. Eng. Perform. 25 (7) (2016) 3057–3064.
[24] Lin Chi-Ming, Chia-Ming Chang, Jie-Hao Chen, Weite Wu, Hardness, toughness and cracking systems of primary $(Cr,Fe)_{23}C_6$ and $(Cr,Fe)_7C_3$ carbides in high-carbon Cr-based alloys by indentation, Mater. Sci. Eng. A 527 (2010) 5038–5043.